UNIVERSITY
OF WOLLONGONG
AUSTRALIA

University of Wollongong
Research Online

Australian Institute for Innovative Materials - Papers

Australian Institute for Innovative Materials

2010

Superconducting properties of carbonaceous chemical doped MgB2

Wenxian Li
University of Wollongong, wenxian@uow.edu.au

S X. Dou
University of Wollongong, shi@uow.edu.au

Publication Details

Li, W & Dou, SX, 2010, Superconducting properties of carbonaceous chemical doped MgB2, In A. Liuz (Eds.), Superconductor, pp. 111-134, Croatia: Sciyo.

Research Online is the open access institutional repository for the University of Wollongong. For further information contact the UOW Library: research-pubs@uow.edu.au

Superconducting properties of carbonaceous chemical doped MgB2

Abstract

The discovery of superconductivity in magnesium diboride (MgB_2: 39 K, in January 2001) (Nagamatsu et al., 2001) has generated enormous interest and excitement in the superconductivity community and the world in general, but especially among researchers into superconductivity in non-oxide and boron related compounds.

Keywords

Superconducting, properties, carbonaceous, chemical, doped, MgB2

Disciplines

Engineering | Physical Sciences and Mathematics

Publication Details

Li, W & Dou, SX, 2010, Superconducting properties of carbonaceous chemical doped MgB2, In A. Liuz (Eds.), Superconductor, pp. 111-134, Croatia: Sciyo.

This journal article is available at Research Online: http://ro.uow.edu.au/aiimpapers/242

6

Superconducting Properties of Carbonaceous Chemical Doped MgB_2

Wenxian Li and Shi-Xue Dou
University of Wollongong
Australia

1. Introduction

The discovery of superconductivity in magnesium diboride (MgB_2: 39 K, in January 2001) (Nagamatsu et al., 2001) has generated enormous interest and excitement in the superconductivity community and the world in general, but especially among researchers into superconductivity in non-oxide and boron related compounds. MgB_2 possesses an AlB_2-type hexagonal structure (space group *P6/mmm*) with alternating boron honeycomb planes and magnesium triangular planes, as shown in Fig. 1. Each Mg atom is located at the center of a hexagon formed by boron, and it donates its electrons to the boron planes; hence, the B-B bonding is strongly anisotropic. The unit cell parameters are a = 0.3086 nm and c = 0.3524 nm at room temperature. These values of lattice parameters for MgB_2 are in the middle of the values of lattice parameters of AlB_2-type compounds. Owing to the simple hexagonal structure with space group *P6/mmm*, four optical modes at the Γ point of the Brillouin zone are predicted for MgB_2 (An & Pickett, 2001): a silent B_{1g} mode (at 87.1 meV, ~700 cm^{-1}), the E_{2g} Raman mode (at 74.5 meV, ~600 cm^{-1}), and the infrared active E_{1u} (at 40.7 meV, ~330 cm^{-1}) and A_{2u} (at 49.8 meV, ~400 cm^{-1}) modes. The E_{2g} mode is responsible for the high transition temperature, T_c, in MgB_2.

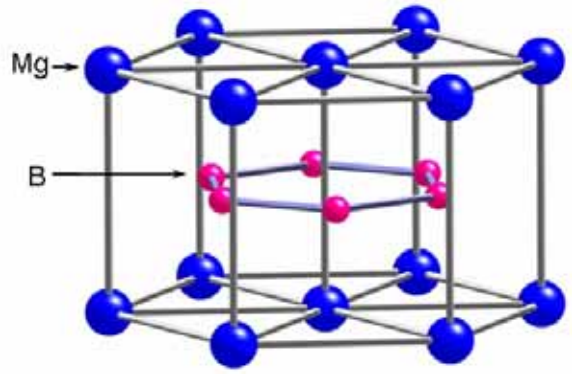

Fig. 1. Hexagonal structure of MgB_2 with space group *P6/mmm* (Nagamatsu et al., 2001)

Further studies based on a number of experimental techniques, such as angle-resolved photoemission spectroscopy (ARPES), the de Haas-van Alphen effect, and Hall resistivity

measurements, have found that MgB_2 exhibits a rich multiple-band structure. These results are in agreement with band structure calculations and reveal strongly two-dimensional $sp_xp_y(\sigma)$ bands, as well as three-dimensional $p_z(\pi)$ bands. The identification of MgB_2 as a two gap superconductor has resulted in much research associated with the spectroscopy of this material. It has become generally accepted that the larger gap is associated with the 2D σ bands arising from the boron planes, which has the value of $\Delta_\sigma \cong 7.069$ meV, while the 3D π bands have a gap of $\Delta_\pi \cong 2.70$ meV (Bouquet et al., 2001; Kortus et al., 2001).

MgB_2 has been fabricated in bulks, single crystals, thin films, tapes, and wires for different applications (Eisterer & Weber, 2009). In addition to the relatively high critical transition temperature, T_c, and the simple crystal structure, MgB_2 possesses a large coherence length, high critical current density, and transparency of grain boundaries to current flow. The *in-situ* route seems to be the most promising method to improve the upper critical field, H_{c2}, and the critical current density, J_c, performance of MgB_2. MgB_2 is a promising superconductor for high-magnetic field applications because of its already high J_c. The grain boundaries in MgB_2 do not significantly degrade J_c and even serve as pinning centers, which is different from the weak-link effects in high-T_c superconductors.

For single-gap dirty limit superconductors, the upper critical field $H_{c2}(0) = 0.69T_c(\mathrm{d}H_{c2}/\mathrm{d}T)_{Tc}$, and $(\mathrm{d}_{Hc2}/\mathrm{d}T)_{Tc} \propto \rho_n$, where ρ_n is the normal state resistivity (Werthame et al., 1966); therefore, H_{c2} increases with ρ_n, which can be achieved by adding impurities and defects into the superconductor. Gurevich pointed out that the two-band superconductor MgB_2 can be understood as a weakly-coupled bilayer in which two thin films corresponding to the σ and π bands are in contact through Josephson coupling (Gurevich, 2007). Using the dirty-limit, weak-coupling, multiband Bardeen Cooper Schrieffer (BCS) model and taking into account both interband and intraband scattering by nonmagnetic impurities, Gurevich showed that the temperature dependence of $H_{c2}(T)$ is influenced by whether the σ bands or π bands are dirtier, making it very different from the temperature dependence in the one-band theory (Gurevich, 2003). The global $H_{c2}(T)$ of the bilayer is dominated by the layer with the higher H_{c2}. If the π layer is dirtier, it will have higher H_{c2} at low temperature, even though its T_c is much lower. As a result, an upturn in the global $H_{c2}(T)$ occurs at low temperature. $H_{c2}(0)$ of MgB_2 can exceed $0.69T_c(\mathrm{d}H_{c2}/\mathrm{d}T)_{Tc}$ considerably because of the existence of the two bands. Considering the electron–phonon coupling effect, Gurevich argued that the strong coupling paramagnetic limit in MgB_2 can be as high as 130 T; thus, there is still room for further enhancement of H_{c2} by engineering the σ- and π-band scattering (Gurevich, 2007). The high H_{c2} in MgB_2 is very attractive for high-magnetic-field applications. The H_{c2} behavior described by Gurevich has been observed in experimental results. For example, Braccini et al. observed different types of temperature dependence of H_{c2}, including the anomalous upturn at low temperature, reflecting different multiband scattering in thin film samples from various groups, with disorder introduced in different ways. The value of H_{c2} in carbon-doped thin films has reached over 60 T at low temperature, approaching the BCS paramagnetic limit of 65 T (Braccini et al., 2005).

The depairing current density, J_d, is ~8.7×10^8 A/cm^2 for pure MgB_2, as estimated from the Ginzburg-Landau (GL) formula:

$$J_d = \Phi_0 / \left[3/\left(\sqrt{3}\right)\pi\mu_0\lambda^2(T)\xi(T) \right] \tag{1}$$

where Φ_0 is the flux quantum, μ_0 the permeability of vacuum, λ the penetration depth, and ξ the coherence length. The self-field critical current density, $J_c(0)$, in the best connected

samples indicates the ultimate current-carrying potential in the superconductor, which has been reported as 3.5×10^7 A/cm^2 at 4.2 K and 1.6×10^8 A/cm^2 at 2 K in clean films made by hybrid physical-chemical vapour deposition (HPCVD). These values are about 4% and 20% of the J_d values. Compared with these values, the $J_c(0)$ values in polycrystalline MgB_2 bulks and wires are very low and have great potential to be improved.

It was pointed out soon after the discovery of MgB_2 that clean grain boundaries are, in principle, no obstacles for supercurrents (Finnemore et al., 2001; Kawano et al., 2001). Such obstacles are known as weak links in the high temperature superconductors. Nevertheless, the connections between the grains remain delicate, since dirty grain boundaries potentially reduce the critical current. Insulating phases have been found at the grain boundaries, consisting of MgO, boron oxides, or boron carbide. Cracks, porosity, or normal conducting phases can further reduce the cross-section over which supercurrents effectively flow. The density of *in-situ* prepared MgB_2 is typically only about half (or less) of its theoretical value, which leads to high porosity.

The *in-situ* route seems to be the most promising method to improve the H_{c2} and J_c performance of MgB_2. Magnesium or MgH_2 reacts with boron after mixing and compacting of these precursor powders. MgB_2 samples with small grains of poor crystallinity can be obtained at low processing temperatures, resulting in strong pinning and high H_{c2}. The stoichiometry can be modified to yield samples with magnesium deficiency, which induces lattice strain, decreases T_c, and increases H_{c2}. An excess of magnesium in the starting powders may compensate the loss of magnesium due to evaporation or due to a reaction with other elements (e.g. with oxygen or with the sheath material). The precursor powders are very important for the properties of the final samples (Yamada et al., 2004). They should be clean to ensure good grain connectivity. The grain size is strongly influenced by the grain sizes of the precursor powders, especially of the boron powders. Ball milling or mechanical alloying of the precursor powders reduces the grain size and improves the critical current.

Chemical or compound doping changes the reaction kinetics and therefore influences the grain growth, the formation of secondary phases, the density, and the stoichiometry. Carbon doping can be easily performed by the addition of B_4C, carbon, carbon nanotubes, nanodiamonds, NbC, SiC, or organic compounds. SiC is by far the most popular dopant, because carbon can be doped into MgB_2 at low temperatures (600 ^oC), according to the dual reaction model (Dou et al., 2007). Higher processing temperatures are necessary for most of the other carbon sources, leading to more grain growth and worse pinning. However, comparable results have also been obtained with nanoscale carbon powder, stearic acid, and carbon nanotubes. It should be noted that the electromagnetic properties of MgB_2 are greatly dependent on the starting materials, shielding metals, processing techniques, and measurements. That is why the irreversibility field (H_{irr}), H_{c2}, and J_c values are different from one batch to another, even for pristine samples, as shown in the figures in this text. All the J_c values are based on the transport measurements reported in this chapter.

2. Nanosized carbon doping effects

The carbon atom has one more electron than boron, and the two-gap feature of MgB_2 can be modified if the extra electron is interposed properly into the system. Fortunately, the carbon atoms show strong substitution effects on the boron sites, both theoretically and experimentally, ranging from 1.225% to 30%. As a result, the enhancement of H_{irr}, H_{c2}, and J_c can be achieved by a controlled carbon doping. The T_c decreases monotonically with

increasing carbon content in the full investigated range of substitution. By adjusting the nominal composition, T_c of substituted crystals can be tuned over a wide temperature range between 10 and 39 K. However, carbon solubility and the effects of carbon doping on T_c vary significantly due to differences in the precursor materials, fabrication techniques, and processing conditions used, because polycrystalline carbon substituted samples may contain significant amounts of impurity phases and the nominal content is assumed most often to be equal to the actual one. Avdeev et al. first suggested the relationship between carbon concentration and lattice parameters. The level of C substitution, x, in the formula $Mg(B_{1-x}C_x)_2$, can be estimated as $x = 7.5\Delta(c/a)$, where $\Delta(c/a)$ is the change in c/a compared to a pure sample (Avdeev et al., 2003).

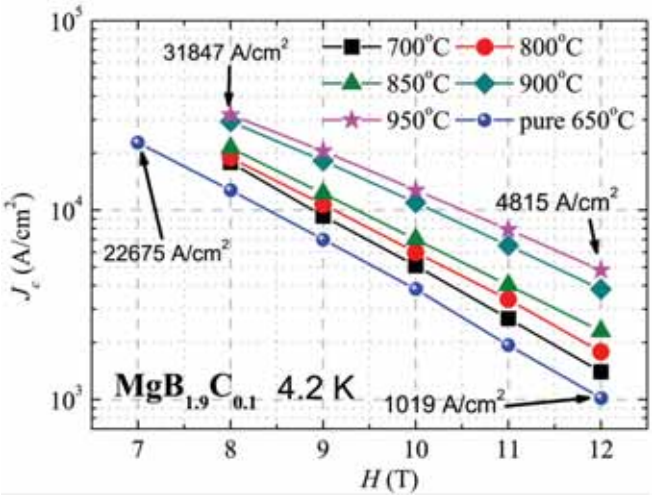

Fig. 2. The effects of sintering temperature on $J_c(H)$ performance of $MgB_{1.9}C_{0.1}$ (Yeoh et al., 2006b)

The J_c performance is greatly dependent on the sintering temperature, as shown in Fig. 2. High sintering temperature is essential for a strong flux pinning force because of the intensive carbon substitution effects. Under the optimum conditions, transport J_c has been enhanced by a factor of 5.7 at 12 T and 4.2 K as compared to the pure MgB_2 wire. The increased H_{c2} shown in Fig. 3 is in agreement with the high carbon substitution effects. $H_{c2}(0)$ of pure MgB_2 increased from 16.0 to 32.5 T in a carbon doped MgB_2 filament with slight depression of T_c from 39.2 to 36.2 K for 3.8% C substitution, using the chemical vapor deposition (CVD) method to co-deposit B together with carbon (Wilke et al., 2004). The carbon substitution effects on H_{c2} have shown an encouraging enhancement, with a range of enhanced H_{c2} values from 25 to 40 T at temperatures of 4.2 K and below (Masui et al., 2004; Ohmichi et al., 2004; Putti et al., 2004). Furthermore, H_{c2} with a value of 52–55 T has been commonly observed for carbon alloyed thin films at temperatures around 1.5–4.2 K (Ferdeghini et al., 2005; Ferrando et al., 2005). The enhancement of H_{c2} is in agreement with predictions of the model of two-band impurity scattering of charge carriers in MgB_2, which indicates increased intraband scattering via shortening of the electron mean free path, l (Gurevich, 2003). The coherence length, ξ, will be shortened according to the equation $1/\xi = 1/l + 1/\xi_0$, where ξ_0 is the coherence length at 0 K.

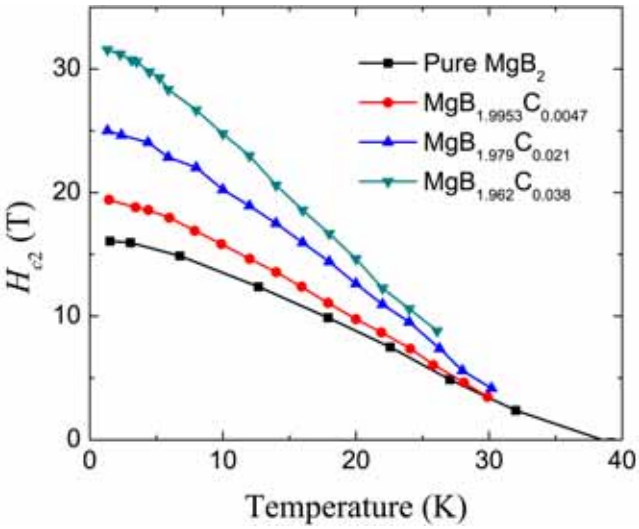

Fig. 3. H_{c2} dependence on carbon substitution content (Wilke et al., 2004)

3. Carbon nanotube (CNT) doping effects

Compared with other nano-carbon precursors, carbon nanotubes (CNTs) are particularly interesting because their special geometry (high aspect ratio and nanometer diameter) may induce more effective pinning centers. CNTs can form column-like strong pinning centers to enhance J_c in the Bi-based superconductors (Fossheim et al., 1995; Huang et al., 1999). The flux pinning force depends greatly on the geometry of the different CNTs. Furthermore, the CNT doping significantly improves heat transfer and dissipation during materials processing (Dou et al., 2006), due to the high thermal conductivity and stable electric conductivity of CNTs (Kim et al., 2001; Wei et al., 2001). With CNT properties of high axial strength and stiffness, approaching values for an ideal carbon fiber (Treacy et al., 1996), CNT doping can improve the current path and connectivity between the grains in MgB_2. Transmission electron microscope (TEM) images have shown that CNTs are easy to align in the wire processing direction, as shown in the TEM images in Fig. 4.

The doping effects of single-walled carbon nanotubes (SWCNTs) include amazing pinning effects in MgB_2 at 4.2 K, as shown in Fig. 4. Similarly to the case of ordinary carbon-doped MgB_2, the best performance in $J_c(H)$ was shown by SWCNT doping with sintering at 900 °C, where the high processing temperature encourages better carbon substitution compared to lower processing temperatures. The J_c(4.2 K) reached the values of ~51,000 and ~3500 A/cm^2 at 7 and 12 T, respectively, as shown in Fig. 5.

Multi-walled carbon nanotubes (MWCNT) have also shown positive effects on the J_c of MgB_2, however, the results are not as significant as with the SWCNTs. Furthermore, the J_c is dependent on the length of the MWCNTs: short MWCNTs give rise to a stronger flux pinning force than long ones. Yeoh et al. have shown that there is a correlation between the reactivity of the CNTs and the amount of carbon substitution in the MgB_2, with the substitution of carbon for boron only occurring after the carbon atoms break free from the CNT (Yeoh et al., 2007a). Longer CNTs tend to entangle and agglomerate, which results in

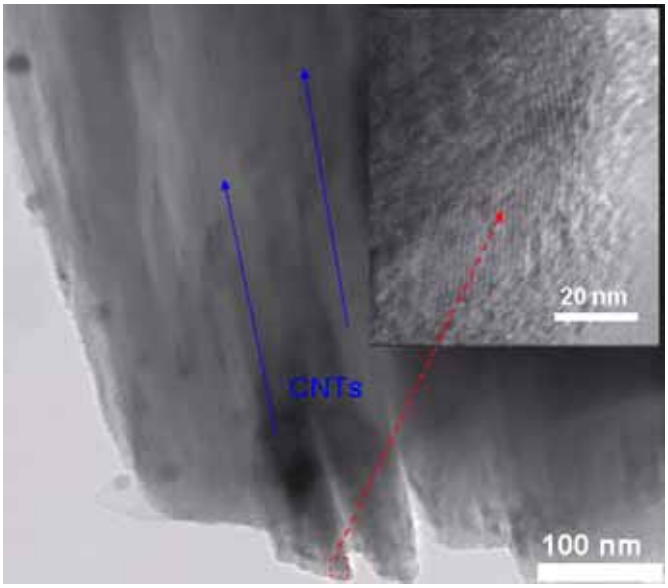

Fig. 4. TEM images of CNT doped MgB_2 show straightened CNTs in the same processing direction in the MgB_2 matrix. The inset is a high resolution image of a CNT (Dou et al., 2006)

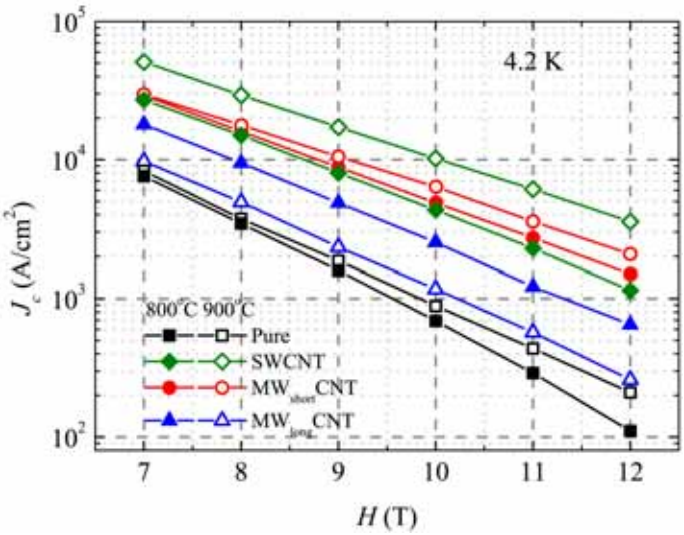

Fig. 5. Transport critical current at 4.2 K at fields up to 12 T for different CNT doped wires produced at sintering temperatures of 800 and 900 °C (Kim et al., 2006a)

inhomogeneous mixing of the CNTs with the precursor powder, blocking the current transport and suppressing the J_c (Yeoh et al., 2005). Ultrasonication of CNTs has been introduced to improve the homogenous mixing of the CNTs with the MgB_2 matrix, resulting in a significant enhancement in the field dependence of the critical current density (Yeoh et

al., 2006a). The J_c performance of different types of CNT doped MgB_2 is in agreement with the H_{c2} shown in Fig. 6.

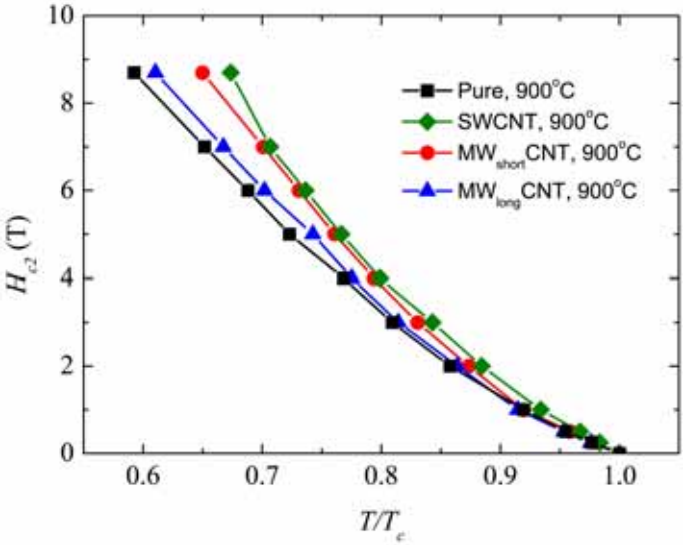

Fig. 6. The H_{c2} of different CNT doped MgB_2 samples sintered at 900 °C. The temperature has been normalized by T_c (Kim et al., 2006a)

4. Nanosized SiC doping effects

Nanosized doping centers are highly effective, as they are comparable with the coherence length of MgB_2 (Soltanian et al., 2003). MgB_2 has a relatively large coherence length, with $\xi_{ab}(0)$ = 3.7–12 nm and $\xi_c(0)$ = 1.6–3.6 nm (Buzea & Yamashita, 2001), so a strong pinning force can be introduced by nanoparticles that are comparable in size. Nanoscale SiC has been found to be the right sort of candidate, providing both second phase nanoscale flux pinning centers and an intensive carbon substitution source (Dou et al., 2002a; Dou et al., 2002b; Dou et al., 2003b). 10 wt% nano-SiC doped MgB_2 bulk samples showed $H_{irr} \approx 8$ T and $J_c \approx 10^5$ A cm^{-2} under 3 T at 20 K. The T_c reduction is not pronounced, even in heavily doped samples with SiC up to 30% (Dou et al., 2002b).

Fig. 7 compares the J_c values of pure MgB_2 and those of MgB_2 doped with 10 wt% nanosized SiC at different temperatures. There are crossover fields for the J_c at the same temperature for different samples, due to the different reductions in slope of the flux pinning force when the temperature is lower than 20 K. The carbon substitution effects in the SiC doped sample are very strong, and therefore, the J_c decreases steadily with increasing field. The J_c drops quickly when the temperature approaches T_c. An increase in H_{c2} from 20.5 T to more than 33 T and enhancement of H_{irr} from 16 T to a maximum of 28 T for an SiC doped sample were observed at 4.2 K (Bhatia et al., 2005). Matsumoto et al. showed that very high values of $H_{c2}(0)$, exceeding 40 T, can be attained in SiC-doped bulk MgB_2 sintered at 600 °C (Matsumoto et al., 2006). This result is considerably higher than for C-doped single crystal (Kazakov et al., 2005), filament (Wilke et al., 2004; Li et al., 2009a), or bulk samples (Senkowicz et al., 2005). Low temperature sintering is beneficial to both the H_{irr} and the H_{c2},

as shown in Fig. 8, which suggests that significant lattice distortion is introduced by alloying and by reaction at low temperature. This has important consequences for the application of MgB_2 wires and tapes in the cable and magnet industries.

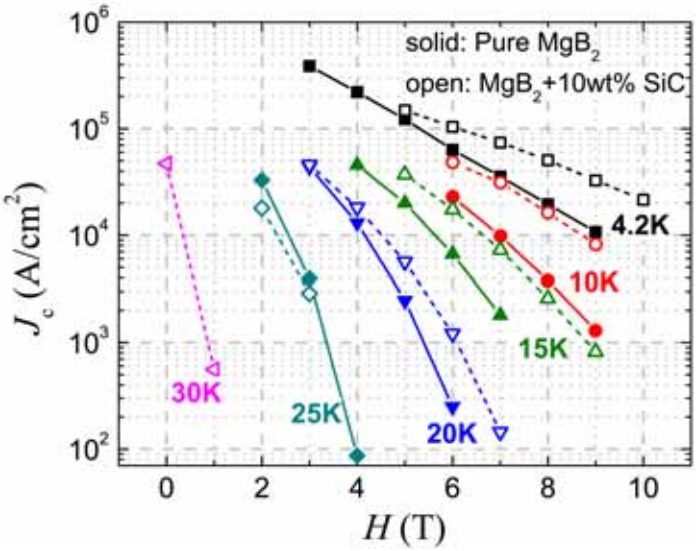

Fig. 7. Comparison of J_c of pure MgB_2 with that of a nanosized SiC doped sample at different temperatures (Dou et al., 2002b; Shcherbakova et al., 2006)

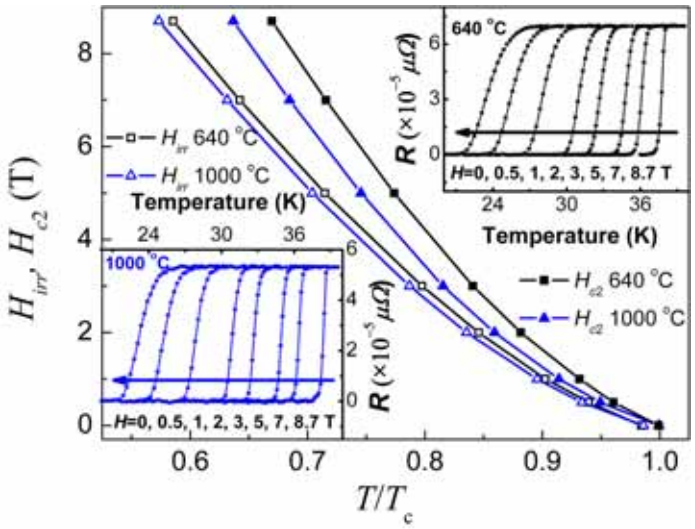

Fig. 8. The effects of sintering temperature on H_{c2} and H_{irr} of 10 wt%, ~15 nm SiC doped MgB_2 (Soltanian et al., 2005). The insets show the resistance as a function of temperature at different magnetic fields for samples sintered at 640 °C (upper right) and 1000 °C (lower left)

Fig. 9 shows the critical current density of MgB_2 in comparison with other commercial superconductor materials. It should be noted that the J_c of SiC-doped MgB_2 stands out very strongly, even at 20 K in low field, and that it is comparable to the value of J_c for Nb–Ti at 4.2 K, which is very useful for application in magnetic resonance imaging (MRI). At 20 K, the best J_c for the 10 wt% SiC doped sample was almost 10^5 A/cm^2 at 3 T, which is comparable with the J_c of state-of-the-art Ag/Bi-2223 tapes. These results indicate that powder-in-tube-processed MgB_2 wire is promising, not only for high-field applications at 4.2 K, but also for applications at 20 K with a convenient cryocooler. Fig. 10 shows TEM and high resolution TEM (HRTEM) images of 10 wt% nanosized SiC doped MgB_2. A high density of dislocations and different sizes of nano-inclusions can be observed in the MgB_2 matrix. Furthermore, the HRTEM images indicate that the MgB_2 crystals display nanodomain structures, which is attributed to lattice collapse caused by the carbon substitution.

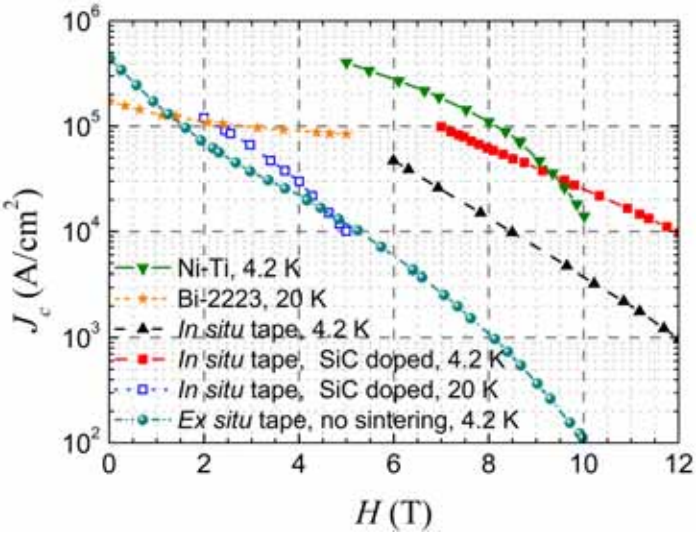

Fig. 9. Comparison of J_c of MgB_2 with those of other commercial superconducting wires and tapes (Yeoh & Dou, 2007)

However, similar to the doping effects of carbon and CNTs, the connectivity of nanosized SiC doped MgB_2 is quite low. To improve the connectivity, additional Mg was added into the precursor mixture (Li et al., 2009a; Li et al., 2009b). To explore the effects on connectivity of Mg excess, microstructures of all the samples were observed by scanning electron microscope (SEM), as shown in Fig. 11. The grains in the stoichiometric MgB_2 samples show an independent growth process, which is responsible for their isolated distribution. The grains in $Mg_{1.15}B_2$ have clearly melted into big clusters because the additional Mg can extend the liquid reaction time. The grain shapes in MgB_2 + 10 wt % SiC are different from those in pure, stoichiometric MgB_2 because the former crystals are grown under strain due to the C substitution effects. The strain is also strong in $Mg_{1.15}B_2$ + 10 wt % SiC, as long bar-shaped grains can be observed under SEM. The strain is released in the high Mg content samples (x > 1.20), judging from the homogeneous grain sizes and shapes. Compared with MgB_2 + 10 wt % SiC, the grain connectivity improved greatly with the increasing Mg addition. The

grains were merged into big particles, and grain boundaries have replaced the gaps between grains. However, more impurities are induced in forms such as residual Mg and MgO.

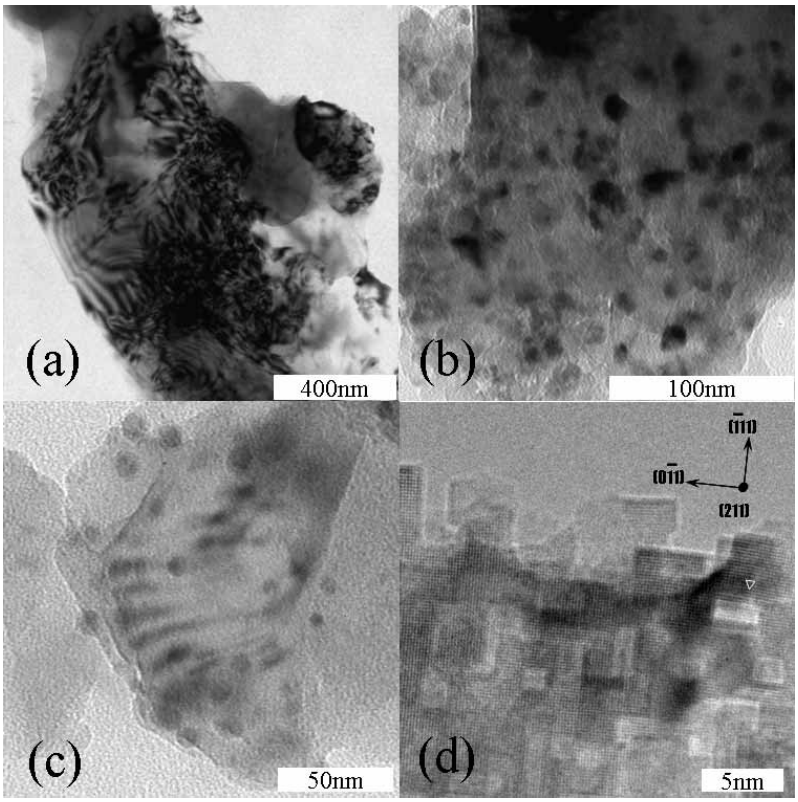

Fig. 10. TEM images of SiC-doped MgB_2 showing the high density of dislocations (a), inclusions larger than 10 nm (b), inclusions smaller than 10 nm (c), and HRTEM image of the nanodomain structure (d) (Dou et al., 2003a; Li et al., 2003)

The concept of the connectivity, A_F, was introduced to quantify this reduction of the effective cross-section, σ_{eff}, for supercurrents (Rowell, 2003; Rowell et al., 2003): $A_F = \sigma_{eff} / \sigma_0$, where σ_0 is the geometrical cross-section. The connectivity can be estimated from the phonon contribution to the normal state resistivity by

$$A_F = \Delta\rho_{\text{ideal}} / \Delta\rho(300\text{ K}) \tag{2}$$

where $\Delta\rho_{\text{ideal}} = \rho_{\text{ideal}}(300\text{ K}) - \rho_{\text{ideal}}(T_c) \approx 9\mu\Omega\cdot\text{cm}$ is the resistivity of fully connected MgB_2 without any disorder, and $\Delta\rho(300\text{ K}) = \rho(300\text{ K}) - \rho(T_c)$. This estimate is based on the assumption that the effective cross-section is reduced equivalently in the normal and superconducting states, which is a severe simplification. The supercurrents are limited by the smallest effective cross-section along the conductor, and the resistivity is given more or less by the average effective cross-section. A single large transverse crack strongly reduces

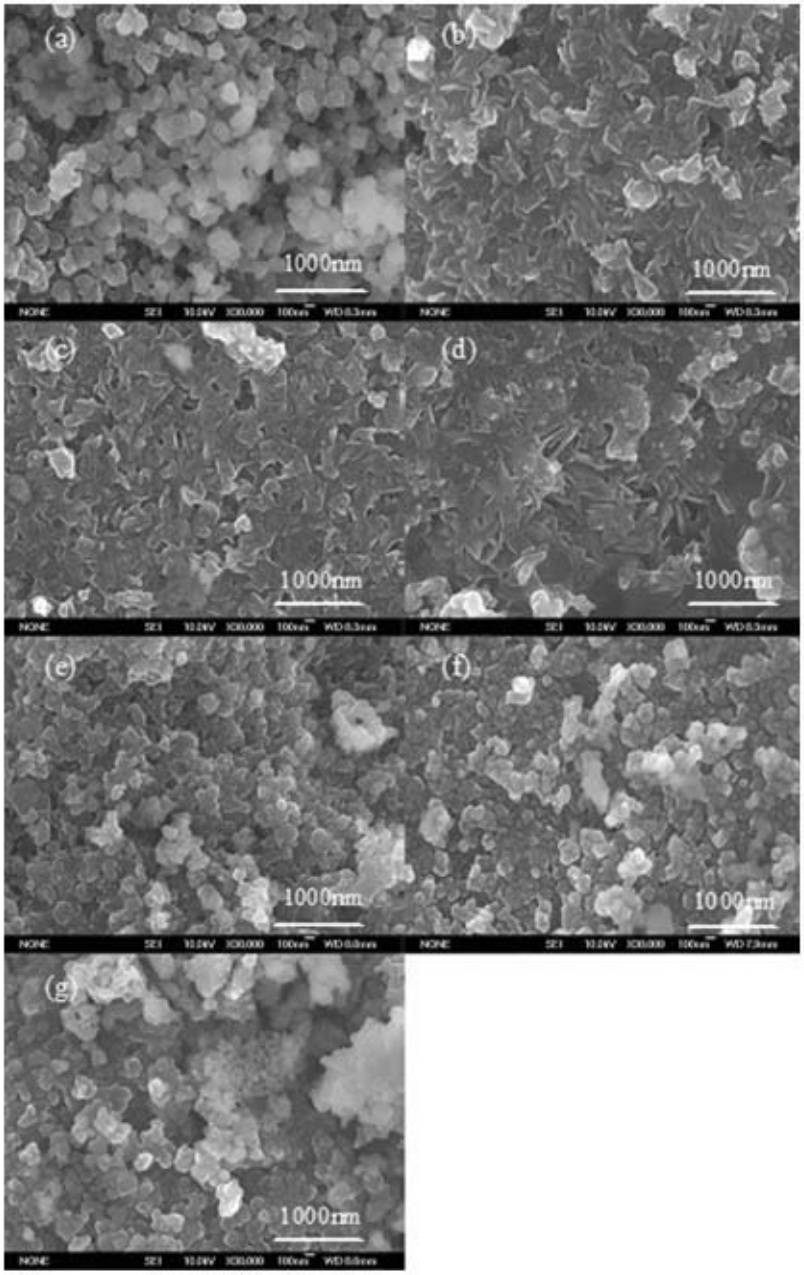

Fig. 11. SEM images of MgB_2 (a), $Mg_{1.15}B_2$ (b), MgB_2+10 wt % SiC (c), $Mg_{1.15}B_2$+10 wt % SiC (d), $Mg_{1.20}B_2$+10 wt % SiC (e), $Mg_{1.25}B_2$+10 wt % SiC (f), and $Mg_{1.30}B_2$+10 wt % SiC (g) (Li et al., 2009a)

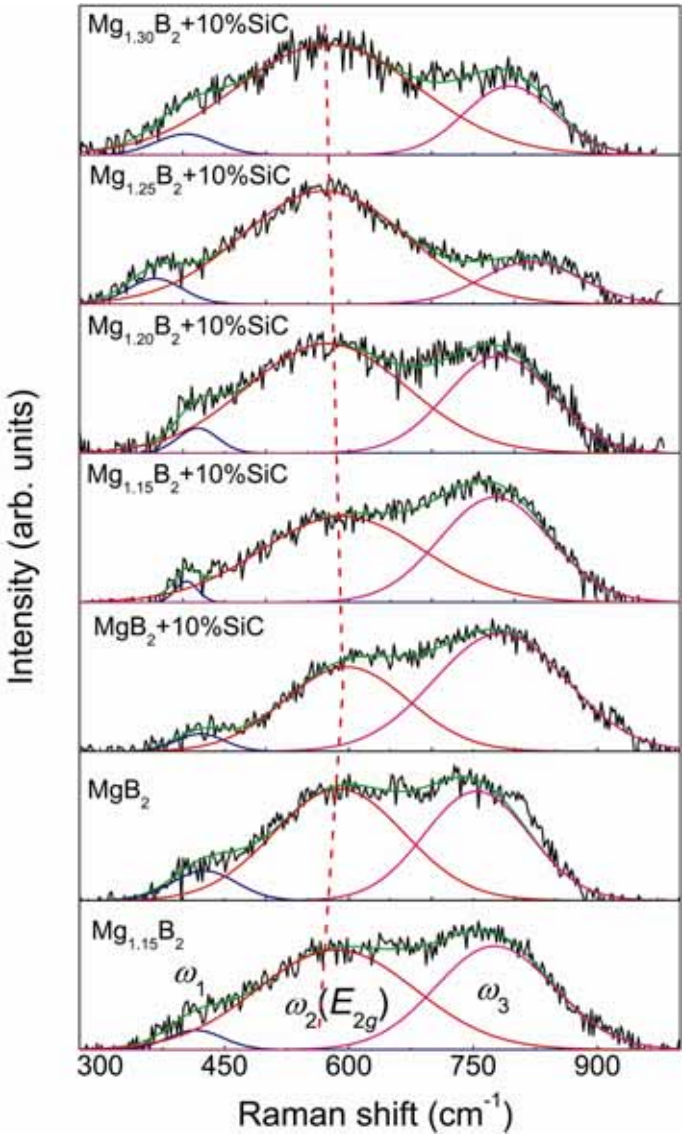

Fig. 12. (Color online) Ambient Raman spectra of MgB_2, $Mg_{1.15}B_2$, and Mg_xB_2+10 wt % SiC (x = 1.00, 1.15, 1.20, 1.25, and 1.30) fitted with three peaks: ω_1, ω_2, and ω_3. The dashed line indicates the vibration of the E_{2g} mode (ω_2) in different samples (Li et al., 2009a)

J_c, but only slightly increases the resistivity of a long sample. Un-reacted magnesium decreases $\Delta\rho$(300 K) (Kim et al., 2002) and the cross-section for supercurrents. Thin insulating layers on the grain boundaries strongly increase $\Delta\rho$(300 K), but might be transparent to supercurrents. Finally, $\Delta\rho_{\text{ideal}}$ within the grains can change due to disorder. Even a negative $\Delta\rho$(300 K) has been reported in highly resistive samples (Sharma et al.,

2002). Despite these objections, A_F is very useful, at least if the resistivity is not too high. A clear correlation between the resistivity and the critical current has been found in thin films (Rowell et al., 2003). Nevertheless, one should be aware of the fact that this procedure is not really reliable, but just a possibility for obtaining an idea about the connectivity.

It should be noted that the connectivity is far removed from that found in ideal crystals, as reflected by the low A_F values. Although the A_F values of pure and 10% SiC doped MgB_2 are just 0.106 and 0.062, additional Mg can improve them to 0.162 and 0.096 for 15 wt % Mg excess samples, respectively. High A_F values are the reflection of a broad channel of supercurrents, while impurities reduce the connectivity in large x samples. High connectivity improves the supercurrent channels because the currents can easily meander through the well-connected grains. The results show that excess Mg in $Mg_{1.15}B_2$ + 10 wt% SiC composite effectively improves the connectivity, as evidenced by its higher A_F. Its promising $J_c(H)$ is attributed to both the high connectivity and the improved H_{irr} and H_{c2}.

Raman scattering is employed to study the combined influence of connectivity and lattice distortion. Chemical substitution and lattice distortion are expected to modify the phonon spectrum, by changing the phonon frequency and the electron-phonon interaction. The effects of C substitution include an increase in impurity scattering and band filling, which reduces the density of states (DOS) and alters the shape of the Fermi surface. The E_{2g} phonon peak shifts to the higher energy side, and the peak is narrowed with increasing x in $Mg(B_{1-x}C_x)_2$ (Li et al., 2008). As a carbon source, nano-SiC shows a similar influence, due to its C atoms, on the J_c, H_{irr}, H_{c2}, and even Raman spectra in MgB_2. Figure 12 shows the Raman spectra fitted with three peaks: ω_1, ω_2, and ω_3. The ω_1 and ω_3 peaks are understood to arise from sampling of the phonon density of states (PDOS) due to disorder, while ω_2 is associated with the E_{2g} mode, which is the only Raman active mode for MgB_2 (Kunc et al., 2001). A reasonable explanation for the appearance of ω_1 and ω_3 is the violation of Raman selection rules induced by disorder. All three peaks are broad, as in previous results, due to the strong electron-phonon coupling. The influence of ω_1 on the superconducting performance is negligible compared with those of ω_2 and ω_3 because of its weak contribution to the Raman spectrum. The frequency and full width at half maximum (FWHM) of ω_2 and ω_3 are shown in Fig. 13. Both ω_2 and ω_3 are hardened with SiC addition. The ω_2 frequency is reduced with further Mg addition, whereas the ω_3 frequency remains almost stable. The frequencies of ω_2 for the $x \geq 1.20$ samples are even lower than for the pure, stoichiometric MgB_2. The FWHM of ω_2 decreases with SiC doping, while the Mg excess weakens this trend. On the contrary, the ω_3 FWHM increases with SiC addition and becomes narrow with more addition of Mg.

The Raman scattering properties are the direct reflection of the phonon behavior of MgB_2. The parameters of Raman spectra vary with the composition of MgB_2 crystals and the influence of their surroundings, which depends on both the connectivity and the disorder of the samples. Furthermore, the disorder should be considered as composed of intrinsic and extrinsic parts based on their different sources. The crystallinity and chemical substitution are believed to be responsible for the intrinsic disorder effects, while the grain boundaries and impurities are treated as responsible for the extrinsic disorder effects. The influences of intrinsic disorder on the basic characteristics of Raman spectra are significant because the physical properties of MgB_2 depend on the intrinsic disorder. The Raman parameters can also be tuned by the extrinsic disorder. Especially in samples with good connectivity, the influences of grain boundaries and impurities on the Raman spectra need to be taken into account because of their strain effects on the MgB_2 crystals (Zeng et al., 2009). The

differences between shifts and FWHMs in the Raman spectra for MgB_2, $Mg_{1.15}B_2$, MgB_2 + 10 wt % SiC, and $Mg_{1.15}B_2$ + 10 wt % SiC are mostly attributable to their intrinsic characteristics because of their different chemical compositions. The Raman spectra of Mg_xB_2 + 10 wt % SiC (x > 1.20) can be considered as gradual modifications of that of $Mg_{1.15}B_2$ + 10 wt % SiC. The weakened C substitution effects are responsible for the decreased frequencies and slightly increased FWHMs of ω_2 with Mg addition. Accordingly, the FWHMs of ω_3 decrease with increased Mg due to the weakened lattice distortion. Although the A_F values are quite low for Mg_xB_2 + 10 wt % SiC (x > 1.20), the effects of extrinsic disorder on Raman parameters are considerable, through the MgB_2–MgB_2 and MgB_2-impurity interfaces, and the connectivity deteriorates with the increased x values due to the decreased number of MgB_2–MgB_2 interfaces. A high FWHM value for ω_2 is correlated with high self-field J_c due to high carrier density, while a high FWHM value for ω_3 is correlated with strong high-field J_c because of the strong flux pinning force due to the large disorder. The FWHM behaviors show that high connectivity and strong disorder are best combined in $Mg_{1.15}B_2$ + 10 wt % SiC among all the samples.

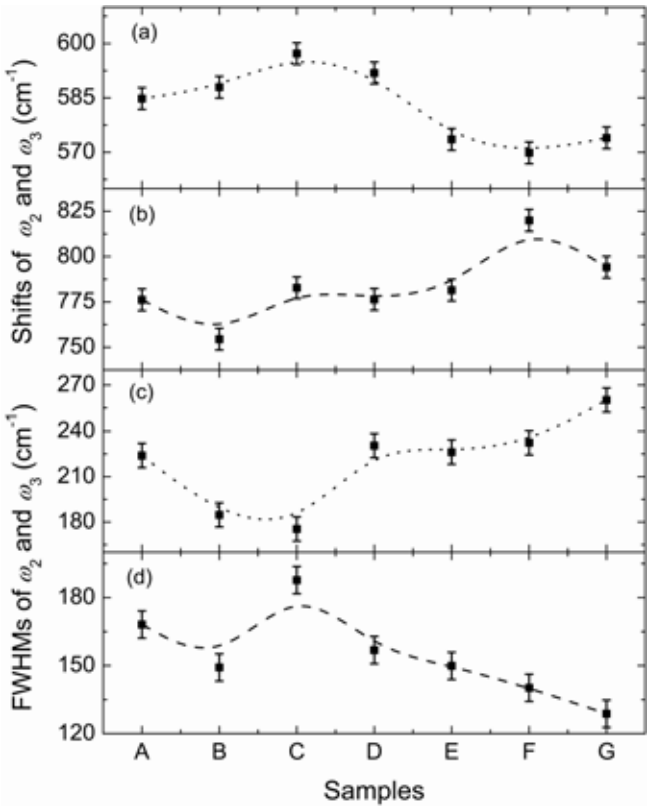

Fig. 13. Fitted parameters of Raman shifts for ω_2 (a) and ω_3 (b), and FWHMs for ω_2 (c) and ω_3 (d). The sample labels are defined as A for $Mg_{1.15}B_2$, B for MgB_2, C for MgB_2+10 wt % SiC, D for $Mg_{1.15}B_2$+10 wt % SiC, E for $Mg_{1.20}B_2$+10 wt % SiC, F for $Mg_{1.25}B_2$+10 wt % SiC, and G for $Mg_{1.30}B_2$+10 wt % SiC (Li et al., 2009a)

5. Organic dopants

Most dopants have been introduced into MgB_2 superconductors via solid state reaction using a dry mixing process, which is responsible for the common inhomogeneous distribution of dopants. Therefore, the soluble nature and low melting point of hydrocarbons and carbohydrates give these dopants advantages over the other carbon based dopants. The homogeneous distribution of hydrocarbons and carbohydrates results in high J_c values comparable with those from the best SiC nanoparticles (Kim et al., 2006b; Yamada et al., 2006; Li et al., 2007; Zhou et al., 2007).

Fig. 14 shows the J_c performance of MgB_2 doped with malic acid and sintered at different temperatures. Low temperature sintering has significant benefits for the J_c. Moreover, the malic acid ($C_4H_6O_5$) doping technique provides additional benefits to the $J_c(H)$ performance in low fields, that is, J_c at low fields is not degraded at certain doping levels as it is for any other C doping method. A cold, high pressure densification technology was employed for improving J_c and H_{irr} of monofilamentary *in-situ* MgB_2 wires and tapes alloyed with 10 wt% $C_4H_6O_5$. Tapes densified at 1.48 GPa exhibited an enhancement of J_c after reaction from 2 to 4 × 10^4 A cm^{-2} at 4.2 K/10 T and from 0.5 to 4 × 10^4 A cm^{-2} at 20 K/5 T, while the H_{irr} was enhanced from 19.3 to 22 T at 4.2 K and from 7.5 to 10.0 T at 20 K (Flukiger et al., 2009; Hossain et al., 2009). Cold densification also caused a strong enhancement of $H(10^4)$, the field at which J_c takes the value 1 × 10^4 A cm^{-2}. For tapes subjected to 1.48 GPa pressure, $H(10^4)||$ and $H(10^4)^{\perp}$ at 4.2 K were found to increase from 11.8 and 10.5 T to 13.2 and 12.2 T, respectively. Almost isotropic conditions were obtained for rectangular wires with aspect ratio a/b < 2 subjected to 2.0 GPa, where $H(10^4)||$ = 12.7 T and $H(10^4)^{\perp}$ = 12.5 T were obtained. At 20 K, the wires exhibited an almost isotropic behavior, with $H(10^4)||$ = 5.9 T and $H(10^4)^{\perp}$ = 5.75 T, with H_{irr}(20 K) being ~10 T. These values are equal to or higher than the highest values reported so far for isotropic *in-situ* wires with SiC or other carbon based additives. Further improvements are expected in optimizing the cold, high pressure densification process, which has the potential for fabrication of MgB_2 wires of industrial lengths.

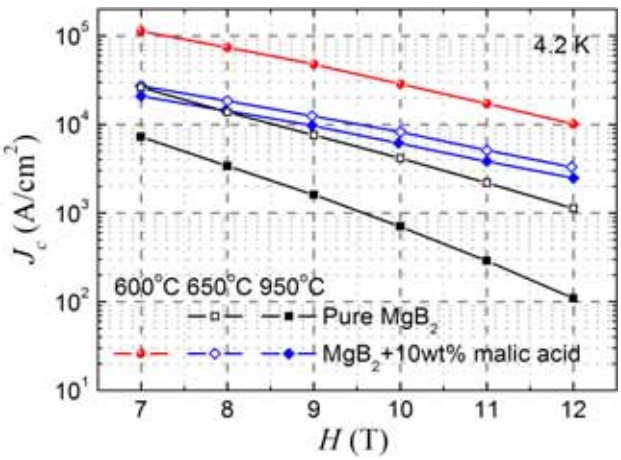

Fig. 14. Sintering temperature effects on the J_c performance of MgB_2 doped with malic acid (Kim et al., 2008)

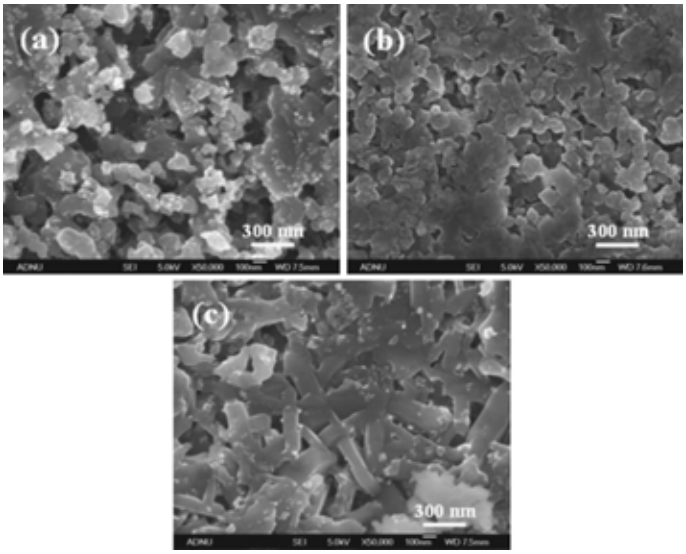

Fig. 15. Field emission SEM images: (a) pure MgB_2, (b) MgB_2 + 10 wt% malic acid, and (c) MgB_2 + 30 wt% malic acid (Kim et al., 2006b)

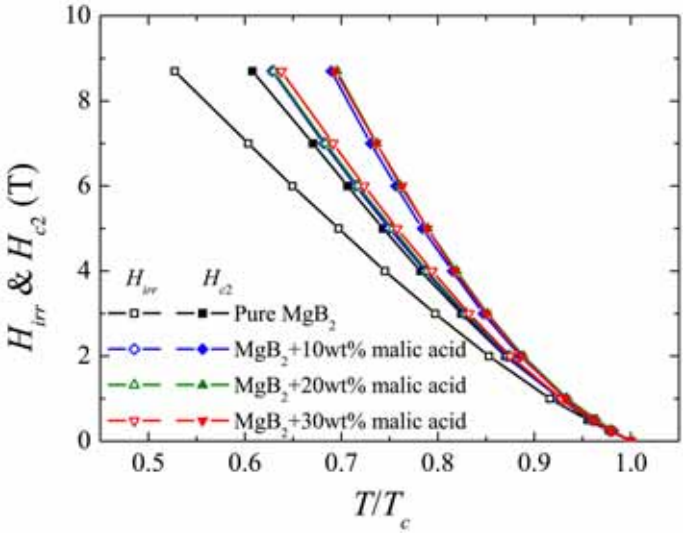

Fig. 16. H_{irr} and H_{c2} variations with doping content of malic acid in MgB_2 (Kim et al., 2006b)

Highly reactive and fresh carbon on the atomic scale can be introduced into the MgB_2 matrix because the organic reagents decompose at temperatures below the formation temperature of MgB_2. The carbon substitution is intensive at temperatures as low as the formation temperature of MgB_2. Microstructural analysis suggests that J_c enhancement is due to the substitution of carbon for boron in MgB_2, liquid homogenous mixing, and highly homogeneous and highly connected MgB_2 grains, as shown in Fig. 15. MgB_2 with

hydrocarbon-based carbonaceous compounds has also demonstrated great application potential due to the improvements in both J_c and H_{c2}, as shown in Fig. 16, while the T_c just decreases slightly. It should be noted that 30 wt% doping with malic acid is still effective for the improvement of H_{c2}, which benefits from the high density of flux pinning centers in the MgB_2 matrix.

6. Doping effects of other carbon sources

Diamond, Na_2CO_3, carbon nanohorns, graphite, and carbide compounds have also been employed as dopants to achieve flux pinning in MgB_2 (Zhao et al., 2003; Ueda et al., 2004; Xu et al., 2004; Ban et al., 2005; Yamamoto et al., 2006). All show positive effects on J_c performance. B_4C appears to be an ideal carbon source to avoid excessive carbonaceous chemical addition. Ueda et al. and Yamamoto et al. showed that C could substitute into the B sites when a mixture of Mg, B, and B_4C was sintered at 850 °C for bulk samples (Ueda et al., 2005; Yamamoto et al., 2005a; Yamamoto et al., 2005c). Substantially enhanced J_c properties under high magnetic fields were observed in the B_4C doped samples due to the relatively low processing temperature and carbon substitution effects. Lezza et al. successfully obtained a J_c value of 1×10^4 A cm^{-2} at 4.2 K and 9 T for 10 wt% B_4C powders added to MgB_2/Fe wires at a reaction temperature of 800 °C (Lezza et al., 2006). Despite the carbon substitution effects, the homogeneous microstructure of the dopants provides the MgB_2 composites with good grain connection for the MgB_2 phase and a high density of flux pinning centers.

7. Mechanism of doping effects — dual reaction model

Carbon substitution in the boron sites is the dominant factor for the enhancement of $J_c(H)$ and H_{c2} in all carbonaceous chemical doped MgB_2 because of the strong disorder effects. Furthermore, the defects, grain sizes, second phases, grain boundaries, and connectivity are also important for the superconducting properties. The study of reaction kinetics for different carbonaceous chemicals during the MgB_2 synthesis is a crucial issue for understanding the H_{irr}, H_{c2}, and J_c performance in MgB_2. A systematic correlation between the processing temperature, J_c, and H_{c2} has been observed in pure, nano-carbon, CNT, SiC, and hydrocarbon doped MgB_2 samples (Dou et al., 2007; Yeoh et al., 2007b). The processing temperature is believed to be the most important factor influencing the electromagnetic properties because both the carbon substitution intensity and the microstructure are dependent on it.

Fig. 17 shows the effects of sintering temperature on the J_c(H) for different carbon based dopants. The hydrocarbon and SiC doped MgB_2 show significant enhancement in J_c for the samples sintered at lower temperature, whereas the carbon and CNT doped MgB_2 need to be sintered at higher temperature for high J_c. The low sintering temperature results in small grain size, high concentrations of impurities and defects, and large lattice distortion, which are all responsible for a strong flux pinning force (Soltanian et al., 2005; Yamamoto et al., 2005b). Furthermore, the hydrocarbon and SiC can release fresh and active free carbon at very low temperature, which means that the carbon substitution effects take place simultaneously with the MgB_2 formation. A high sintering temperature will perfect the crystallization and decrease the flux pinning centers in the MgB_2 matrix. That is the reason why high sintering temperature degrades the J_c performance. Although high sintering

temperature has the same shortcomings in nanosized carbon and CNT doped MgB_2, the carbon substitution effects improve their J_c values. The high sintering temperature is necessary for carbon and CNT doped MgB_2 because the carbon and CNT are quite stable at low temperature and the substitution effects are absent if the sintering temperature is not high enough.

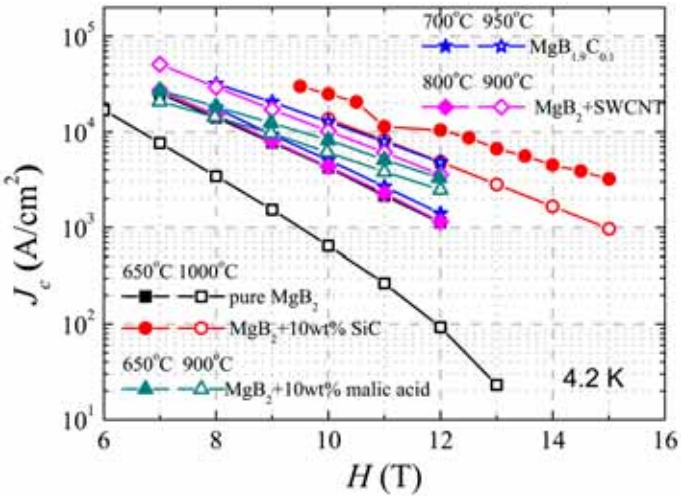

Fig. 17. The critical current density (J_c) at 4.2 K versus magnetic field for wires of pure MgB_2 and MgB_2 doped with C, SiC, SWCNTs, and malic acid that were sintered at different temperatures (Dou et al., 2002b; Yeoh et al., 2006b; Dou et al., 2007; Kim et al., 2008)

A dual reaction model has been suggested to explain the improvement of the superconducting properties in SiC doped MgB_2, based on the J_c dependence on the sintering temperature (Dou et al., 2007). The reaction of SiC with Mg at low temperature will release fresh and active carbon, which is easily incorporated into the lattice of MgB_2 at the same temperature. The reaction product Mg_2Si and excess carbon are also high quality nanosized flux pinning centers. The low temperature substitution is accompanied by small grain size, high density of grain boundaries, and high density of all kinds of defects, which are all favorable to the high superconducting performance. Another example for the dual reaction model is the high J_c malic acid doped MgB_2 shown in Fig. 14. The carbonaceous chemical doping effects on the superconducting performance can be predicted according to the dual reaction model as arising from the combination of defects and carbon substitution effects. Most dopants, such as TiC and NbC, show very small effects towards the enhancement of J_c compared with carbon, SiC, CNTs, and hydrocarbons because the substitution effects are very weak and there are no efficient flux pinning centers either.

8. Conclusions

The experimental results on H_{c2} and J_c strongly suggest that MgB_2 doped with carbonaceous sources shows remarkable enhancement of superconducting performance if the carbon substitution effects are intensive. In particular, nanosized SiC and malic acid are the most promising dopants to advance the high field J_c performance for practical application. The

enhancement of J_c, H_{irr}, and H_{c2} for MgB_2 with carbon substituted into boron sites is due to its intrinsic properties arising from the strong two-band impurity scattering effects of charge carriers. The carbonaceous chemical doping effects have been attributed to a dual reaction model, based on the sintering effects on superconducting properties for different kinds of carbonaceous chemicals. The fresh, active, and free carbon atoms are very easy to substitute onto B sites in the MgB_2 lattice if the carbonaceous decomposition temperatures are close to the formation temperature of MgB_2, ~650 °C. The dual reaction model can explain and predict the doping effects of carbonaceous chemicals on the superconducting properties very well. The high density of defects is another factor that improves the J_c, H_{irr}, and H_{c2}. However, the connectivity of the samples is also responsible for the low field J_c performance, which is free from the flux pinning force and can be attributed to the density of supercurrent carriers. Both microstructure observations and Raman scattering measurements have confirmed the great influence of connectivity on J_c behavior, as shown by the effects of extra Mg addition in nanosized SiC doped MgB_2. The proper Mg content will improve the connectivity greatly to improve the density of supercurrent carriers.

9. References

An, J. M. & Pickett, W. E. (2001). Superconductivity of MgB_2: Covalent bonds driven metallic. *Physical Review Letters*, 86(19): 4366-4369.

Avdeev, M.; Jorgensen, J. D.; Ribeiro, R. A.; Bud'ko, S. L. & Canfield, P. C. (2003). Crystal chemistry of carbon-substituted MgB_2. *Physica C - Superconductivity and Its Applications*, 387(3-4): 301-306.

Ban, E.; Sakaguchi, R.; Matsuoka, Y.; Goto, T.; Watanabe, K. & Nishijima, G. (2005). Carbon nanohorn doping in MgB_2 wire prepared by suspension spinning. *Physica C - Superconductivity and Its Applications*, 426-431(9): 1249-1253.

Bhatia, M.; Sumption, M. D. & Collings, E. W. (2005). Effect of various additions on upper critical field and irreversibility field of *in-situ* MgB_2 superconducting bulk material. *IEEE Transactions on Applied Superconductivity*, 15(2): 3204-3206.

Bouquet, F.; Fisher, R. A.; Phillips, N. E.; Hinks, D. G. & Jorgensen, J. D. (2001). Specific heat of (MgB_2)-^{11}B: Evidence for a second energy cap. *Physical Review Letters*, 87(4): 047001.

Braccini, V.; Gurevich, A.; Giencke, J. E.; Jewell, M. C.; Eom, C. B.; Larbalestier, D. C.; Pogrebnyakov, A.; Cui, Y.; Liu, B. T.; Hu, Y. F.; Redwing, J. M.; Li, Q.; Xi, X. X.; Singh, R. K.; Gandikota, R.; Kim, J.; Wilkens, B.; Newman, N.; Rowell, J.; Moeckly, B.; Ferrando, V.; Tarantini, C.; Marre, D.; Putti, M.; Ferdeghini, C.; Vaglio, R. & Haanappel, E. (2005). High-field superconductivity in alloyed MgB_2 thin films. *Physical Review B*, 71(1): 012504.

Buzea, C. & Yamashita, T. (2001). Review of the superconducting properties of MgB_2. *Superconductor Science & Technology*, 14(11): R115-R146.

Dou, S. X.; Horvat, J.; Soltanian, S.; Wang, X. L.; Qin, M. J.; Zhou, S. H.; Liu, H. K. & Munroe, P. G. (2003a). Transport critical current density in Fe-sheathed nano-SiC doped MgB_2 wires. *IEEE Transactions on Applied Superconductivity*, 13(2): 3199-3202.

Dou, S. X.; Pan, A. V.; Zhou, S.; Ionescu, M.; Liu, H. K. & Munroe, P. R. (2002a). Substitution-induced pinning in MgB_2 superconductor doped with SiC nano-particles. *Superconductor Science & Technology*, 15(11): 1587-1591.

Dou, S. X.; Pan, A. V.; Zhou, S.; Ionescu, M.; Wang, X. L.; Horvat, J.; Liu, H. K. & Munroe, P. R. (2003b). Superconductivity, critical current density, and flux pinning in $MgB_{2-x}(SiC)_{x/2}$ superconductor after SiC nanoparticle doping. *Journal of Applied Physics*, 94(3): 1850-1856.

Dou, S. X.; Shcherbakova, O.; Yoeh, W. K.; Kim, J. H.; Soltanian, S.; Wang, X. L.; Senatore, C.; Flukiger, R.; Dhalle, M.; Husnjak, O. & Babic, E. (2007). Mechanism of enhancement in electromagnetic properties of MgB_2 by nano SiC doping. *Physical Review Letters*, 98(9): 097002.

Dou, S. X.; Soltanian, S.; Horvat, J.; Wang, X. L.; Zhou, S. H.; Ionescu, M.; Liu, H. K.; Munroe, P. & Tomsic, M. (2002b). Enhancement of the critical current density and flux pinning of MgB_2 superconductor by nanoparticle SiC doping. *Applied Physics Letters*, 81(18): 3419-3421.

Dou, S. X.; Yeoh, W. K.; Shcherbakova, O.; Weyler, D.; Li, Y.; Ren, Z. M.; Munroe, P.; Chen, S. K.; Tan, K. S.; Glowacki, B. A. & MacManus-Driscoll, J. L. (2006). Alignment of carbon nanotube additives for improved performance of magnesium diboride superconductors. *Advanced Materials*, 18(6): 785-788.

Eisterer, M. & Weber, H. W. (2009). Application prospects of MgB_2 in view of its basic properties. *IEEE Transactions on Applied Superconductivity*, 19(3): 2788-2792.

Ferdeghini, C.; Ferrando, V.; Tarantini, C.; Bellingeri, E.; Grasso, G.; Malagoli, A.; Marre, D.; Putti, M.; Manfrinetti, P.; Pogrebnyakov, A.; Redwing, J. M.; Xi, X. X.; Felici, R. & Haanappel, E. (2005). Upper critical fields up to 60 T in dirty magnesium diboride thin films. *IEEE Transactions on Applied Superconductivity*, 15(2): 3234-3237.

Ferrando, V.; Orgiani, P.; Pogrebnyakov, A. V.; Chen, J.; Li, Q.; Redwing, J. M.; Xi, X. X.; Giencke, J. E.; Eom, C. B.; Feng, Q. R.; Betts, J. B. & Mielke, C. H. (2005). High upper critical field and irreversibility field in MgB_2 coated-conductor fibers. *Applied Physics Letters*, 87(25): 252509.

Finnemore, D. K.; Ostenson, J. E.; Bud'ko, S. L.; Lapertot, G. & Canfield, P. C. (2001). Thermodynamic and transport properties of superconducting MgB_2-^{10}B. *Physical Review Letters*, 86(11): 2420-2422.

Flukiger, R.; Hossain, M. S. A. & Senatore, C. (2009). Strong enhancement of J_c and B_{irr} in binary *in situ* MgB_2 wires after cold high pressure densification. *Superconductor Science & Technology*, 22(8): 085002.

Fossheim, K.; Tuset, E. D.; Ebbesen, T. W.; Treacy, M. M. J. & Schwartz, J. (1995). Enhanced flux-pinning in $Bi_2Sr_2CaCu_2O_{8+X}$ superconductor with embedded carbon nanotubes. *Physica C - Superconductivity and Its Applications*, 248(3-4): 195-202.

Gurevich, A. (2003). Enhancement of the upper critical field by nonmagnetic impurities in dirty two-gap superconductors. *Physical Review B*, 67(18): 184515.

Gurevich, A. (2007). Limits of the upper critical field in dirty two-gap superconductors. *Physica C - Superconductivity and Its Applications*, 456(1-2): 160-169.

Hossain, M. S. A.; Senatore, C.; Flukiger, R.; Rindfleisch, M. A.; Tomsic, M. J.; Kim, J. H. & Dou, S. X. (2009). The enhanced J_c and B_{irr} of in situ MgB_2 wires and tapes alloyed with $C_4H_6O_5$ (malic acid) after cold high pressure densification. *Superconductor Science & Technology*, 22(9): 095004.

Huang, S. L.; Koblischka, M. R.; Fossheim, K.; Ebbesen, T. W. & Johansen, T. H. (1999). Microstructure and flux distribution in both pure and carbon-nanotube-embedded

$Bi_2Sr_2CaCu_2O_{8+\delta}$ superconductors. *Physica C - Superconductivity and Its Applications*, 311(3-4): 172-186.

Kawano, K.; Abell, J. S.; Kambara, M.; Babu, N. H. & Cardwell, D. A. (2001). Evidence for high intergranular current flow in a single-phase polycrystalline MgB_2 superconductor. *Applied Physics Letters*, 79(14): 2216-2218.

Kazakov, S. M.; Puzniak, R.; Rogacki, K.; Mironov, A. V.; Zhigadlo, N. D.; Jun, J.; Soltmann, C.; Batlogg, B. & Karpinski, J. (2005). Carbon substitution in MgB_2 single crystals: Structural and superconducting properties. *Physical Review B*, 71(2): 024533.

Kim, J. H.; Dou, S. X.; Oh, S.; Jercinovic, M.; Babic, E.; Nakane, T. & Kumakura, H. (2008). Correlation between doping induced disorder and superconducting properties in carbohydrate doped MgB_2. *Journal of Applied Physics*, 104(6): 063911.

Kim, J. H.; Yeoh, W. K.; Qin, M. J.; Xu, X.; Dou, S. X.; Munroe, P.; Kumakura, H.; Nakane, T. & Jiang, C. H. (2006a). Enhancement of in-field J_c in MgB_2/Fe wire using single- and multiwalled carbon nanotubes. *Applied Physics Letters*, 89(12): 122510.

Kim, J. H.; Zhou, S.; Hossain, M. S. A.; Pan, A. V. & Dou, S. X. (2006b). Carbohydrate doping to enhance electromagnetic properties of MgB_2 superconductors. *Applied Physics Letters*, 89(14): 142505.

Kim, K. H.; Betts, J. B.; Jaime, M.; Lacerda, A. H.; Boebinger, G. S.; Jung, C. U.; Kim, H. J.; Park, M. S. & Lee, S. I. (2002). Mg as a main source for the diverse magnetotransport properties of MgB_2. *Physical Review B*, 66(2): 020506.

Kim, P.; Shi, L.; Majumdar, A. & McEuen, P. L. (2001). Thermal transport measurements of individual multiwalled nanotubes. *Physical Review Letters*, 87(21): 215502.

Kortus, J.; Mazin, I. I.; Belashchenko, K. D.; Antropov, V. P. & Boyer, L. L. (2001). Superconductivity of metallic boron in MgB_2. *Physical Review Letters*, 86(20): 4656-4659.

Kunc, K.; Loa, I.; Syassen, K.; Kremer, R. K. & Ahn, K. (2001). MgB_2 under pressure: phonon calculations, Raman spectroscopy, and optical reflectance. *Journal of Physics - Condensed Matter*, 13(44): 9945-9962.

Lezza, P.; Senatore, C. & Flukiger, R. (2006). Improved critical current densities in B_4C doped MgB_2 based wires. *Superconductor Science & Technology*, 19(10): 1030-1033.

Li, S.; White, T.; Laursen, K.; Tan, T. T.; Sun, C. Q.; Dong, Z. L.; Li, Y.; Zhou, S. H.; Horvat, J. & Dou, S. X. (2003). Intense vortex pinning enhanced by semicrystalline defect traps in self-aligned nanostructured MgB_2. *Applied Physics Letters*, 83(2): 314-316.

Li, W. X.; Li, Y.; Chen, R. H.; Zeng, R.; Dou, S. X.; Zhu, M. Y. & Jin, H. M. (2008). Raman study of element doping effects on the superconductivity of MgB_2. *Physical Review B*, 77(9): 094517.

Li, W. X.; Li, Y.; Zhu, M. Y.; Chen, R. H.; Xu, X.; Yeoh, W. K.; Kim, J. H. & Dou, S. X. (2007). Benzoic acid doping to enhance electromagnetic properties of MgB_2 superconductors. *IEEE Transactions on Applied Superconductivity*, 17(2): 2778-2781.

Li, W. X.; Zeng, R.; Lu, L.; Li, Y. & Dou, S. X. (2009a). The combined influence of connectivity and disorder on J_c and T_c performances in Mg_xB_2+10 wt % SiC. *Journal of Applied Physics*, 106(9): 093906.

Li, W. X.; Zeng, R.; Lu, L.; Zhang, Y.; Dou, S. X.; Li, Y.; Chen, R. H. & Zhu, M. Y. (2009b). Improved superconducting properties of in situ powder-in-tube processed $Mg_{1.15}B_2$/Fe wires with nano-size SiC addition. *Physica C - Superconductivity and Its Applications*, 469(15-20): 1519-1522.

Masui, T.; Lee, S. & Tajima, S. (2004). Carbon-substitution effect on the electronic properties of MgB_2 single crystals. *Physical Review B*, 70(2): 024504.

Matsumoto, A.; Kumakura, H.; Kitaguchi, H.; Senkowicz, B. J.; Jewell, M. C.; Hellstrom, E. E.; Zhu, Y.; Voyles, P. M. & Larbalestier, D. C. (2006). Evaluation of connectivity, flux pinning, and upper critical field contributions to the critical current density of bulk pure and SiC-alloyed MgB_2. *Applied Physics Letters*, 89(13): 132508.

Nagamatsu, J.; Nakagawa, N.; Muranaka, T.; Zenitani, Y. & Akimitsu, J. (2001). Superconductivity at 39 K in magnesium diboride. *Nature*, 410(6824): 63-64.

Ohmichi, E.; Komatsu, E.; Masui, T.; Lee, S.; Tajima, S. & Osada, T. (2004). Carbon-substitution effect on vortex order-disorder transition in MgB_2 single crystals. *Physical Review B*, 70(17): 174513.

Putti, M.; Braccini, V.; Ferdeghini, C.; Pallecchi, I.; Siri, A. S.; Gatti, F.; Manfrinetti, P. & Palenzona, A. (2004). Critical field of MgB_2: Crossover from clean to dirty regimes. *Physical Review B*, 70(5): 052509.

Rowell, J. M. (2003). The widely variable resistivity of MgB_2 samples. *Superconductor Science & Technology*, 16(6): R17-R27.

Rowell, J. M.; Xu, S. Y.; Zeng, H.; Pogrebnyakov, A. V.; Li, Q.; Xi, X. X.; Redwing, J. M.; Tian, W. & Pan, X. Q. (2003). Critical current density and resistivity of MgB_2 films. *Applied Physics Letters*, 83(1): 102-104.

Senkowicz, B. J.; Giencke, J. E.; Patnaik, S.; Eom, C. B.; Hellstrom, E. E. & Larbalestier, D. C. (2005). Improved upper critical field in bulk-form magnesium diboride by mechanical alloying with carbon. *Applied Physics Letters*, 86(20): 202502.

Sharma, P. A.; Hur, N.; Horibe, Y.; Chen, C. H.; Kim, B. G.; Guha, S.; Cieplak, M. Z. & Cheong, S. W. (2002). Percolative superconductivity in $Mg_{1-x}B_2$. *Physical Review Letters*, 89(16): 167003.

Shcherbakova, O.; Dou, S. X.; Soltanian, S.; Wexler, D.; Bhatia, M.; Sumption, M. & Collings, E. W. (2006). The effect of doping level and sintering temperature on $J_c(H)$ performance in nano-SiC doped and pure MgB_2 wires. *Journal of Applied Physics*, 99(8): 08M510.

Soltanian, S.; Wang, X. L.; Horvat, J.; Dou, S. X.; Sumption, M. D.; Bhatia, M.; Collings, E. W.; Munroe, P. & Tomsic, M. (2005). High transport critical current density and large H_{c2} and H_{irr} in nanoscale SiC doped MgB_2 wires sintered at low temperature. *Superconductor Science & Technology*, 18(5): 658-666.

Soltanian, S.; Wang, X. L.; Horvat, J.; Qin, M. J.; Liu, H. K.; Munroe, P. R. & Dou, S. X. (2003). Effect of grain size and doping level of SiC on the superconductivity and critical current density in MgB_2 superconductor. *IEEE Transactions on Applied Superconductivity*, 13(2): 3273-3276.

Treacy, M. M. J.; Ebbesen, T. W. & Gibson, J. M. (1996). Exceptionally high Young's modulus observed for individual carbon nanotubes. *Nature*, 381(6584): 678-680.

Ueda, S.; Shimoyama, J.; Yamamoto, A.; Katsura, Y.; Iwayama, I.; Horii, S. & Kishio, K. (2005). Flux pinning properties of impurity doped MgB_2 bulks synthesized by diffusion method. *Physica C-Superconductivity and Its Applications*, 426-431(2): 1225-1230.

Ueda, S.; Shimoyama, J. I.; Yamamoto, A.; Horii, S. & Kishio, K. (2004). Enhanced critical current properties observed in Na_2CO_3-doped MgB_2. *Superconductor Science & Technology*, 17(7): 926-930.

Wei, B. Q.; Vajtai, R. & Ajayan, P. M. (2001). Reliability and current carrying capacity of carbon nanotubes. *Applied Physics Letters*, 79(8): 1172-1174.

Werthame, N. R.; Helfand, E. & Hohenber, P. C. (1966). Temperature and purity dependence of the superconducting critical field, H_{c2}. III. Electron spin and spin-orbit effects. *Physical Review*, 147(1): 295-302.

Wilke, R. H. T.; Bud'ko, S. L.; Canfield, P. C.; Finnemore, D. K.; Suplinskas, R. J. & Hannahs, S. T. (2004). Systematic effects of carbon doping on the superconducting properties of $Mg(B_{1-x}C_x)_2$. *Physical Review Letters*, 92(21): 217003.

Xu, H. L.; Feng, Y.; Xu, Z.; Yan, G.; Cao, L. Z. & Li, X. G. (2004). Enhancement of critical current density in graphite doped MgB_2 wires. *Chinese Physics Letters*, 21(12): 2511-2513.

Yamada, H.; Hirakawa, M.; Kumakura, H. & Kitaguchi, H. (2006). Effect of aromatic hydrocarbon addition on in situ powder-in-tube processed MgB_2 tapes. *Superconductor Science & Technology*, 19(2): 175-177.

Yamada, H.; Hirakawa, M.; Kumakura, H.; Matsumoto, A. & Kitaguchi, H. (2004). Critical current densities of powder-in-tube MgB_2 tapes fabricated with nanometer-size Mg powder. *Applied Physics Letters*, 84(10): 1728-1730.

Yamamoto, A.; Shimoyama, J.; Ueda, S.; Horii, S. & Kishio, K. (2006). Reactivity of carbides in synthesis of MgB_2 bulks. *Physica C - Superconductivity and Its Applications*, 445-448: 801-805.

Yamamoto, A.; Shimoyama, J.; Ueda, S.; Iwayama, I.; Horii, S. & Kishio, K. (2005a). Effects of B_4C doping on critical current properties of MgB_2 superconductor. *Superconductor Science & Technology*, 18(10): 1323-1328.

Yamamoto, A.; Shimoyama, J.; Ueda, S.; Katsura, Y.; Iwayama, I.; Horii, S. & Kishio, K. (2005b). Universal relationship between crystallinity and irreversibility field of MgB_2. *Applied Physics Letters*, 86(21): 212502.

Yamamoto, A.; Shimoyama, J. I.; Ueda, S.; Katsura, Y.; Horii, S. & Kishio, K. (2005c). Doping effects on critical current properties of MgB_2 bulks synthesized by modified powder-in-tube method. *IEEE Transactions on Applied Superconductivity*, 15(2): 3292-3295.

Yeoh, W. K. & Dou, S. (2007). Enhancement of H_{c2} and J_c by carbon-based chemical doping. *Physica C - Superconductivity and Its Applications*, 456(1-2): 170-179.

Yeoh, W. K.; Horvat, J.; Dou, S. X. & Munroe, P. (2005). Effect of carbon nanotube size on superconductivity properties of MgB_2. *IEEE Transactions on Applied Superconductivity*, 15(2): 3284-3287.

Yeoh, W. K.; Horvat, J.; Kim, J. H.; Xu, X. & Dou, S. X. (2007a). Effect of carbon substitution on the superconducting properties of MgB_2 doped with multi-walled carbon nanotubes and nano carbon. *IEEE Transactions on Applied Superconductivity*, 17(2): 2929-2932.

Yeoh, W. K.; Horvat, J.; Kim, J. H.; Xu, X. & Dou, S. X. (2007b). Effect of processing temperature on high field critical current density and upper critical field of nanocarbon doped MgB_2. *Applied Physics Letters*, 90(12): 122502.

Yeoh, W. K.; Kim, J. H.; Horvat, J.; Dou, S. X. & Munroe, P. (2006a). Improving flux pinning of MgB_2 by carbon nanotube doping and ultrasonication. *Superconductor Science & Technology*, 19(2): L5-L8.

Yeoh, W. K.; Kim, J. H.; Horvat, J.; Xu, X.; Qin, M. J.; Dou, S. X.; Jiang, C. H.; Nakane, T.; Kumakura, H. & Munroe, P. (2006b). Control of nano carbon substitution for enhancing the critical current density in MgB_2. *Superconductor Science & Technology*, 19(6): 596-599.

Zeng, R.; Dou, S. X.; Lu, L.; Li, W. X.; Kim, J. H.; Munroe, P.; Zheng, R. K. & Ringer, S. P. (2009). Thermal-strain-induced enhancement of electromagnetic properties of SiC-MgB_2 composites. *Applied Physics Letters*, 94(4): 042510.

Zhao, Y.; Cheng, C. H.; Rui, X. F.; Zhang, H.; Munroe, P.; Zeng, H. M.; Koshizuka, N. & Murakami, M. (2003). Improved irreversibility behavior and critical current density in MgB_2-diamond nanocomposites. *Applied Physics Letters*, 83(14): 2916-2918.

Zhou, S. H.; Pan, A. V.; Wexler, D. & Dou, S. X. (2007). Sugar coating of boron powder for efficient carbon doping of MgB_2 with enhanced current-carrying performance. *Advanced Materials*, 19(10): 1373-1376.